Clostridium difficile toxin B-induced necrosis is mediated by the host epithelial cell NADPH oxidase complex

Melissa A. Farrow[a], Nicole M. Chumbler[b], Lynne A. Lapierre[c,d], Jeffrey L. Franklin[d,e,f], Stacey A. Rutherford[a], James R. Goldenring[c,d,e,f,g], and D. Borden Lacy[a,1]

[a]Department of Pathology, Microbiology, and Immunology, [b]Chemical and Physical Biology Program, [c]Department of Surgery, [d]Epithelial Biology Center, [e]Department of Medicine, and [f]Department of Cell and Developmental Biology, Vanderbilt University School of Medicine, Nashville, TN 37232; and [g]Nashville Veterans Affairs Medical Center, Nashville, TN 37232

Edited by R. John Collier, Harvard Medical School, Boston, MA, and approved October 11, 2013 (received for review July 19, 2013)

Clostridium difficile **infection (CDI) is a leading cause of health care-associated diarrhea and has increased in incidence and severity over the last decade. Pathogenesis is mediated by two toxins, TcdA and TcdB, which cause fluid secretion, inflammation, and necrosis of the colonic mucosa. TcdB is a potent cytotoxin capable of inducing enzyme-independent necrosis in both cells and tissue. In this study, we show that TcdB-induced cell death depends on assembly of the host epithelial cell NADPH oxidase (NOX) complex and the production of reactive oxygen species (ROS). Treating cells with siRNAs directed against key components of the NOX complex, chemical inhibitors of NOX function, or molecules that scavenge superoxide or ROS confers protection against toxin challenge. To test the hypothesis that chemical inhibition of TcdB-induced cytotoxicity can protect against TcdB-induced tissue damage, we treated colonic explants with diphenyleneiodonium (DPI), a flavoenzyme inhibitor, or *N*-acetylcysteine (NAC), an antioxidant. TcdB-induced ROS production in colonic tissue was inhibited with DPI, and both DPI and NAC conferred protection against TcdB-induced tissue damage. The efficacy of DPI and NAC provides proof of concept that chemical attenuation of ROS could serve as a viable strategy for protecting the colonic mucosa of patients with CDI.**

Clostridium difficile is the most prevalent cause of antibiotic-associated diarrhea and pseudomembranous colitis worldwide (1–3). The majority of pathogenic strains secrete two large exotoxins, TcdA and TcdB, which are responsible for the massive fluid secretion, colonic tissue necrosis, and inflammation associated with disease (4). These toxins are homologs and share 48% amino acid identity, although they appear to have nonredundant and potentially synergistic functions in pathogenesis (5, 6).

TcdA and TcdB are large (308 kDa and 270 kDa, respectively) glucosyltransferases that modify Rho and Ras family GTPases within the cell (7, 8). The C-terminal portion of these toxins is responsible for delivering the N-terminal glucosyltransferase domain into the host cell (9). Monoglucosylation of RhoA, Rac1, and Cdc42 disrupts the actin cytoskeleton and causes a cytopathic "rounding" effect in toxin-treated cells (10). In addition to the cytopathic effect, TcdB is a potent cytotoxin, ∼1,000 times more potent than TcdA in most cell lines (11, 12). Multiple studies have demonstrated that TcdA and TcdB have different binding activities, suggesting that the toxins have distinct receptors (12–15). Defining the relative contributions of TcdA and TcdB in pathogenesis, as well as the impact of the cytopathic and cytotoxic effects, is an active area of investigation.

Our laboratory has recently shown that TcdB induces rapid cell death in both human colonic cell lines and porcine colonic explants (16). The death mechanism has been characterized as necrotic based on rapid ATP depletion, observed loss of membrane integrity, lack of caspase-3/7 activation, and rapid lactate dehydrogenase (LDH) and HMGB1 release. The necrosis is independent of the TcdB auto processing and glucosyltransferase functions and occurs at concentrations predicted to be relevant in the context of CDI (16).

The present study was designed to define the molecular mechanism of TcdB-mediated necrotic cell death. We report the unexpected involvement of the NADPH oxidase (NOX) complex and the potential for exploiting this mechanistic knowledge for therapeutic intervention.

Results

The observation that TcdB can induce necrosis in a glucosyltransferase- and autoprocessing-independent manner (16) led us to investigate what aspects of TcdB are important for induction of cell death. Although we knew that the enzymatic modification of GTPase targets is not required, we could not exclude the possibility of the GTPases playing other roles in the cell death response. To test this possibility, we used an siRNA approach to knock down RhoA, Rac1, and Cdc42 transcripts in HeLa and Caco2 epithelial cells. A siRNA pool directed against the clathrin heavy chain (CLTC) was included as a positive control, because TcdB is internalized by clathrin-mediated endocytosis (17), and a siRNA pool directed to luciferase (Luc) was included as a negative control. Cells were challenged with TcdB, and cytotoxicity was assessed with CellTiterGlo, an ATP viability indicator (Fig. 1*A*).

The RhoA and Cdc42 knockdowns did not demonstrate a statistically significant protective phenotype in either cell type compared with negative control cells (Luc siRNA). Interestingly, we observed significant protection from cytotoxicity, equivalent to CLTC knockdown, when Rac1 was silenced in either HeLa or

Significance

The toxin-producing bacterium *Clostridium difficile* is the leading cause of antibiotic-associated infection in hospitals worldwide. An estimated 500,000 cases of *C. difficile* infection (CDI) occur annually in the US, with a cost approaching 3 billion dollars. The principle virulence factors in *C. difficile* pathogenesis are TcdA and TcdB, two large homologous toxins capable of entering host cells to cause fluid secretion, inflammation, and necrosis of the colonic mucosa. Given that numerous investigators are currently targeting these toxins for the development of novel CDI therapies, understanding the mechanism of toxicity is a significant priority.

Author contributions: M.A.F., J.R.G., and D.B.L. designed research; M.A.F., N.M.C., L.A.L., J.L.F., and S.A.R. performed research; M.A.F., N.M.C., L.A.L., J.L.F., J.R.G., and D.B.L. analyzed data; and M.A.F. and D.B.L. wrote the paper.

The authors declare no conflict of interest.

This article is a PNAS Direct Submission.

[1]To whom correspondence should be addressed. E-mail: borden.lacy@vanderbilt.edu.

This article contains supporting information online at www.pnas.org/lookup/suppl/doi:10.1073/pnas.1313658110/-/DCSupplemental.

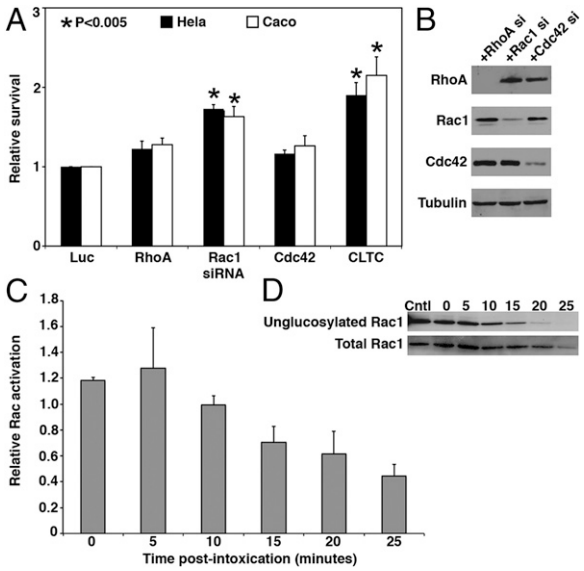

Fig. 1. TcdB cytotoxicity depends on Rac1. (*A*) HeLa (black) or Caco-2 (white) cells transfected with siRNA for 48 h were challenged with 50 nM TcdB for 16 h. Signals were internally normalized against mock-treated controls. Relative survival is a normalized signal compared with a Luc siRNA control. CLTC knockdown was included as a positive control. Error bars represent SE. *P* values were determined by the Student *t* test and are relative to the Luc control. The Rac1 and CLTC knockdowns were statistically different from Luc ($P < 0.005$), but not statistically significantly different from one another ($P > 0.05$). (*B*) HeLa cells transfected with GTPase siRNA for 48 h were lysed, and protein levels for RhoA, Rac1, or Cdc42 were assessed by Western blot analysis. Tubulin was included as a loading control. (*C*) HeLa cells were incubated with 10 nM toxin, and Rac1 activation was quantified using the G-LISA Assay Kit over 5-min intervals. Relative activation was calculated by comparison with a mock-treated control at the same time point. Data represent the average of three experiments; error bars represent SEs. (*D*) HeLa cells were treated with 10 nM toxin, and Rac1 glucosylation was determined by Western blot analysis over 5-min intervals. Levels of unglucosylated and total Rac1 were determined by probing with Rac1-specific antibodies.

Caco2 cells. Because RhoA, Rac1, and Cdc42 are closely related and serve functionally redundant roles in some cellular processes, we confirmed the specificity of knockdown by monitoring protein levels (Fig. 1*B*). These data suggest that TcdB cytotoxicity is mediated by a Rac1-dependent pathway.

The observation that Rac1 is required for cytotoxicity (Fig. 1*A*) when TcdB is known to inactivate Rac1 by glucosylation led us to investigate the kinetics of Rac1 activation and inactivation in response to TcdB. Rac1 activation was quantified every 5 min for 25 min after TcdB treatment using the G-LISA Assay Kit (Cytoskeleton) (Fig. 1*C*). A transient activation of Rac1 was detected immediately on toxin binding, with peak activation occurring at 5 min postintoxication (Fig. 1*C*). Subsequently, Rac1 became inactivated, as indicated by the loss of ability to bind to a downstream effector.

To assess the timing of Rac1 glucosylation, we probed lysates from the TcdB-treated cells with an antibody that recognizes only unglucosylated forms of Rac1. We found that Rac1 modification begins at 10 min and is completed by 25 min postintoxication (Fig. 1*D*). Our data are consistent with a hypothesis in which the Rac1 activation required for the cell death response occurs faster than the process through which toxin is delivered to the cytosol to enzymatically inactivate Rac1 by glycosylation.

Recent reports have revealed a critical role for Rac1 in the assembly of NADPH oxidase (NOX) complexes in nonphagocytic cells (18). The prototypical NOX complex comprises the membrane-associated gp91phox and p22phox subunits, as well as the cytosolic p47phox and p67phox subunits (19). Assembly of a functional complex is dependent on Rac1 binding to the cytosolic subunits, thereby mediating association with the membrane-bound components. On receptor-mediated membrane invagination and endocytosis, the NOX complexes give rise to redox active endosomes that generate superoxide and then reactive oxygen species (ROS) (20). ROS have been shown to cause pleiotropic effects ranging from prosurvival signals or the induction of apoptotic cascades with moderate levels of ROS to more severe outcomes, such as mitochondrial damage, lipid peroxidation, and protein oxidation, with higher levels of ROS (21). Given that the severe outcomes are associated with necrotic cell death, we investigated NOX-mediated ROS production as a possible mechanism to explain TcdB-mediated necrosis.

To test whether TcdB could induce intracellular ROS, we used an intracellular, fluorescent ROS reporter and challenged cells with toxins. TcdB treatment induced an intense signal, indicating a robust ROS response approaching the level seen with exogenous application of H_2O_2 (Fig. 2*A*). The ROS response was specific to TcdB; stimulation with TcdA did not generate comparable ROS production (Fig. 2*A*). This finding is consistent with our observation that TcdA does not induce rapid necrosis in HeLa cells (16). The glucosyltransferase-impaired TcdB D270N mutant (16) and WT TcdB were equipotent in the ROS assay, demonstrating that ROS production in response to TcdB is a glucosyltransferase-independent process (Fig. 2*A*). This observation is consistent with relative survival data (Fig. 2*B*) and our previous study showing that TcdB-induced necrosis does not depend on glucosyltransferase activity (16).

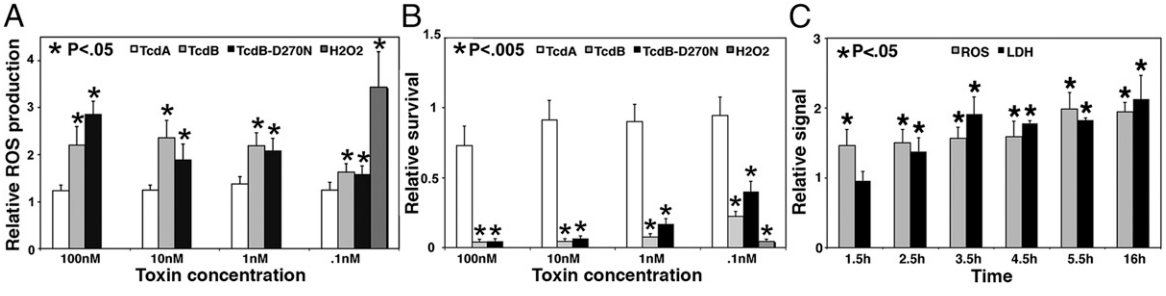

Fig. 2. TcdB induces ROS production. (*A*) HeLa cells treated with the indicated concentrations of TcdA, TcdB, or TcdB-D270N or with 1 mM H_2O_2 for 16 h were analyzed for ROS production in a plate-based assay. Relative ROS production is a measure of ROS compared with a mock- treated control. (*B*) HeLa cells (shown in *A*) were assessed for cytotoxicity of each treatment and normalized to a mock-treated control. (*C*) HeLa cells treated with 10 nM toxin were assayed for ROS production and LDH release starting at 1.5 h postintoxication. ROS production and LDH release are relative to mock-treated controls. Error bars represent SE. *P* values were calculated by the Student *t* test and are relative to mock-treated controls.

Decreasing the concentration of TcdB resulted in decreased ROS production (Fig. 2*A*) and increased cell viability (Fig. 2*B*), suggesting that these phenotypes are inversely correlated. Time course experiments indicated that whereas ROS was detectable within 1.5 h postintoxication, LDH release (a marker of necrosis) was not detectable until 2.5 h postintoxication (Fig. 2*C*). The early production of ROS followed by LDH release is consistent with previous observations of rapid cell death in response to TcdB (16), and clearly establishes the sequence of ROS production preceding cell death.

ROS are produced from various sources in metabolically active cells. To distinguish NOX-derived ROS from other potential ROS sources, we took a genetic ablation approach. The NOX pathway is best characterized in the "respiratory burst" of phagocytic cells in which the gp91phox (NOX2) and p22phox membrane subunits associate (22). In nonphagocytic cells, the NOX2 homologs NOX1, NOX3, and NOX4 interact with p22phox to form the catalytic core of the NOX complex (23, 24).

To address the question of whether NOX-derived ROS contribute to TcdB-mediated cell death, NOX1–4 and p22phox were individually targeted with siRNA pools and challenged with TcdB in both HeLa and Caco2 cells (Fig. 3*A*). In HeLa cells, NOX3 and p22phox knockdowns conferred significant protection against toxin challenge. Caco2 cells also showed a strong protective phenotype for the p22phox knockdown, but NOX1, rather than NOX3, appeared to be responsible for most of the response. The specificity for different NOX homologs can be explained by cell line-specific differences in the NOX expression profiles (Fig. 3*B*). NOX1 is the predominant form in Caco2 cells, whereas NOX3 is the most highly expressed NOX in HeLa cells. In both HeLa and Caco2, knockdown of the prevalent NOX isoform and p22phox provides significant protection against toxin challenge, demonstrating a clear role for the NOX complex in toxin-mediated cell death.

The protective phenotypes of Rac1 (Fig. 1*A*) and p22phox knockdown (Fig. 3*A*) coupled with the TcdB-induced ROS shown in Fig. 2*A* suggest that TcdB cytotoxicity is the result of NOX-mediated ROS production. To confirm that toxin-induced ROS production depends on Rac1 and p22phox, we performed simultaneous viability and ROS detection assays in the context of siRNA knockdown of Rac1 or p22phox (Fig. 3*C*). This multiplexed assay showed that relative to the Luc siRNA negative control, knockdown of either p22phox or Rac1 with siRNA leads to decreased ROS production and increased survival in response to TcdB. These changes in ROS and viability are comparable to the ROS production and survival observed in the clathrin siRNA-positive control (Fig. 3*C*). The inverse correlation of Rac1 or p22phox expression and ROS production in response to toxin indicates activation of a NOX-dependent pathway on toxin stimulation.

To extend these findings, we used pharmacologic reagents that prevent ROS production or act as either antioxidants or scavengers in toxin challenge assays. Diphenyleneiodonium (DPI) and NSC 23766 exert their effects upstream of ROS generation by inhibiting the flavocytochrome enzymatic core of the NOX complex (DPI) or inhibiting a Rac1 guanine nucleotide exchange factor (NSC 23766). *N*-acetylcysteine (NAC) is an antioxidant, and Tempol is a superoxide scavenger. HeLa cells were treated with a compound or a mock control before being challenged with toxin. For each compound, viability was assayed and compared with the mock control (Fig. 3*D*). Either inhibiting the generation of ROS or scavenging ROS free radicals was sufficient to protect cells from TcdB-induced necrosis. Taken together, the data presented in Figs. 1, 2, and 3 demonstrate that TcdB-induced activation of the NOX complex leads to ROS production and ultimately cell death.

We next wanted to assess whether ROS are produced in the context of colonic tissue, and whether DPI and NAC can confer protection against TcdB-mediated tissue damage. Porcine colonic explants were treated with the ROS indicator dye in the presence or absence of 10 μM DPI. Tissue was then challenged with 10 nM toxin for 5 h and then flash-frozen. Tissue challenged with 10 nM toxin showed a robust induction of ROS relative to untreated controls (Fig. 4*A*). ROS were attenuated in tissues pretreated with DPI.

In addition, similarly treated tissues were fixed, stained with H&E (Fig. 4*B*) or keratin (Fig. 4*C*), and assessed for signs of damage in the surface epithelial layer. Tissues treated with 10 nM TcdB in the absence of DPI showed extensive damage in the surface epithelial layer. Increasing the dose to 100 nM toxin resulted

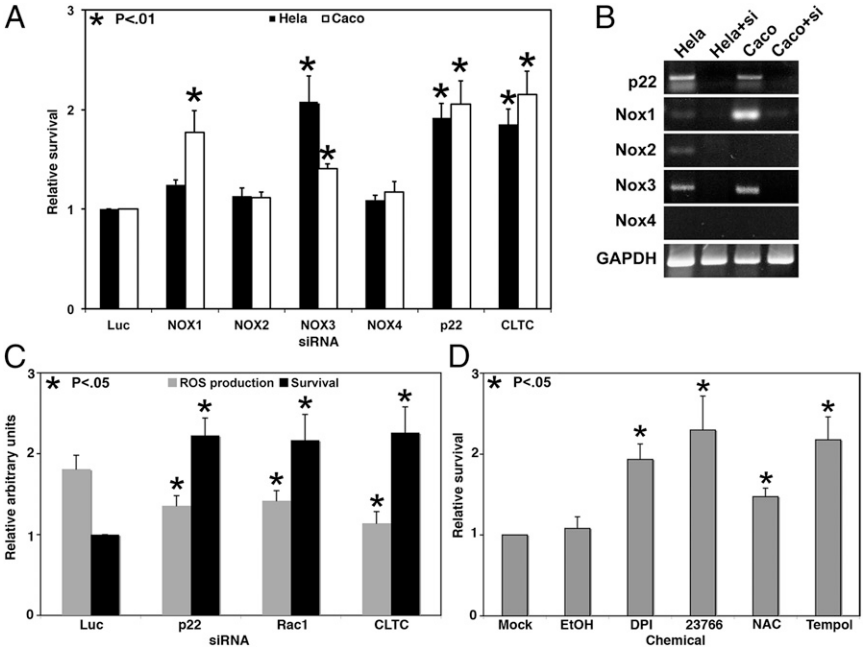

Fig. 3. NOX inhibition confers protection against TcdB cytotoxicity. (*A*) NOX family members were targeted with siRNA in HeLa (black) or Caco2 (white) cells for 48 h before challenge with 50 nM TcdB for 16 h. Signals were internally normalized against mock-treated controls. Relative survival is a normalized signal compared with a Luc negative control. CLTC knockdown was included as a positive control. Error bars represent SE. *P* values are relative to the Luc control. (*B*) The expression profile and knockdown efficiency of each siRNA in HeLa or Caco2 was determined by RT-PCR for the specified transcript in the presence or absence of siRNA. Amplification of GAPDH by RT-PCR served as an RNA loading control. (*C*) The p22phox and Rac1 siRNAs were transfected into HeLa cells for 48 h before challenge with 50 nM TcdB for 16 h, after which cells were assayed for ROS and viability. ROS production for each treatment was internally normalized to mock-treated cells and is shown relative to Luc. Viability is normalized and shown relative to Luc. Error bars represent SE. *P* values are relative to the Luc control. (*D*) HeLa cells were pretreated with ROS inhibitors for 1 h and then challenged with 10 nM TcdB for 16 h. Viability was measured and normalized to mock-treated samples. Error bars represent SE. *P* values are relative to mock-treated controls.

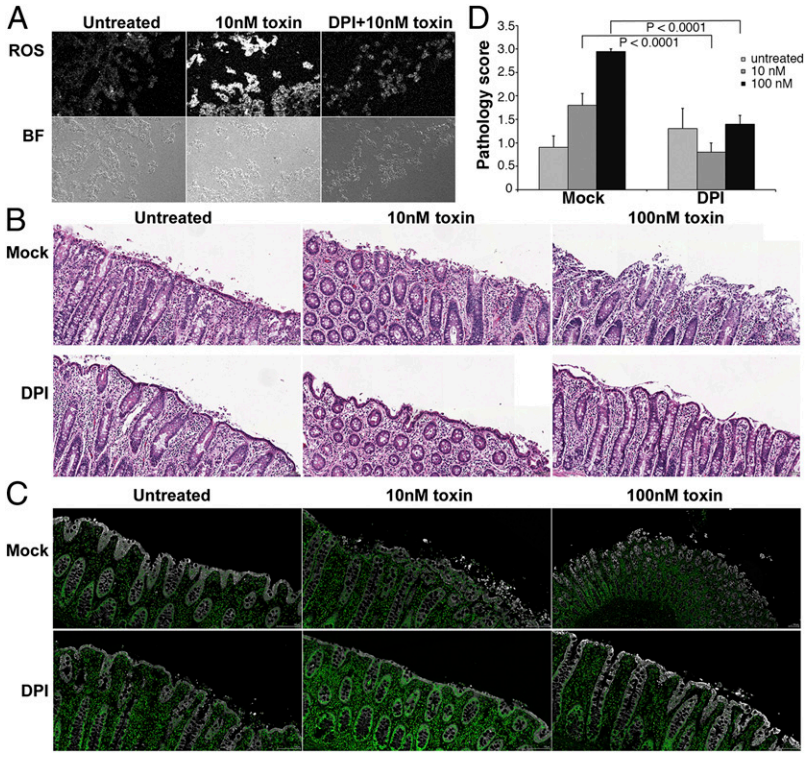

Fig. 4. Toxin induces ROS in colonic explants. (*A*) Porcine colonic explants were incubated with ROS detection reagent and simultaneously received either mock treatment or 10 μM DPI for 1 h. Tissue was treated with 10 nM TcdB for 5 h, and fresh-frozen sections were prepared. ROS production was detected with a confocal microscope. Representative sections for ROS and brightfield (BF) are shown. (*B*) Tissue was mock-treated or treated with 10 μM DPI for 1 h. Then 10 nM or 100 nM toxin was applied for 5 h, and sections were stained with H&E. The surface epithelium is apparent as a contiguous layer in intact tissue. Loss of tissue architecture is apparent when surface epithelium is denuded and underlying epithelium becomes disorganized. (Scale bar: 100 μm.) (*C*) Tissue sections shown in *B* were stained with keratin (white) and DAPI (green), and images were scanned. Keratin staining is apparent on the epithelial surface, and disruption correlates with tissue damage. (Scale bar: 100 μm.) (*D*) Pathology scores are the mean scores for sections evaluated independently by five individuals in a blinded fashion. Statistical analysis was performed with two-way ANOVA and post hoc tests, which revealed a significant difference in the intoxicated mock-treated versus DPI-treated tissues ($P < 0.0001$).

in further damage to the surface and extensive damage throughout the tissue. DPI maintained the integrity of the tissue when challenged with a 10 nM or 100 nM toxin dose (Fig. 4*D*). The maintenance of tissue architecture and reduced ROS production on exposure to DPI demonstrates the key contribution of ROS production to TcdB-induced colonic tissue necrosis.

The abrogation of ROS production and concomitant preservation of tissue architecture in porcine colonic explants treated with DPI points to ROS attenuation as a potential strategy for protecting the colonic mucosa in patients with CDI. As a flavocytochrome inhibitor, DPI is expected to be toxic, however. Consequently, we wished to extend our studies to human colonic explants and to evaluate the efficacy of NAC, a Food and Drug Administration-approved antioxidant. In this assay, human colonic explants were treated with NAC for 1 h before a challenge with 10 nM or 100 nM toxin. Tissues stained with H&E (Fig. 5*A*) were assessed for damage to the colonic epithelium (Fig. 5*B*). Similar to what was observed in the porcine model, treating human colonic tissue with 10 nM or 100 nM TcdB caused significant damage to the surface epithelial layer (Fig. 5*A*, *Upper*); however, NAC treatment conferred protection against toxin-induced damage (Fig. 5*A*, *Lower*). Quantification and statistical analysis of pathology scores revealed significant damage in tissues treated with 10 nM or 100 nM toxin compared with control tissue. Although some damage did occur in the NAC-treated samples, it was severely attenuated compared with that in mock-treated tissue. The ability of antioxidant treatment to confer protection against TcdB in a human colonic explant model further highlights the importance of ROS production in TcdB-induced necrosis.

Discussion

This study was designed to define the mechanism of TcdB-induced necrosis. A recent study in our laboratory indicated that necrosis occurs through an autoprocessing- and glucosyltransferase-independent mechanism and suggested that the Rho family

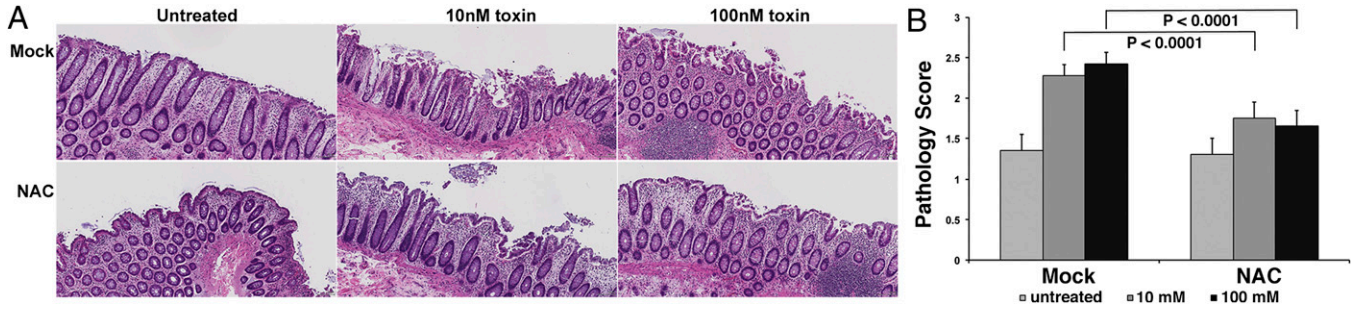

Fig. 5. NAC attenuates TcdB-mediated damage in human colonic explants. (*A*) Human colonic explant tissue was mock-treated or pretreated with NAC for 1 h before treatment with 10 nM or 100 nM TcdB. Tissue was fixed for 3 h postintoxication and sections were stained with H&E. (Scale bar: 100 μm.) (*B*) Pathology scores were assigned using a semiquantitative injury scale as in Fig. 4. Average scores shown are the mean score for sections evaluated independently by five individuals. Statistical analysis performed with two-way ANOVA and post hoc tests revealed a significant difference in the intoxicated mock-treated versus NAC-treated tissues ($P < 0.0001$).

GTPases (targets of the TcdB glucosyltransferase domain) might not be involved in the cell death pathway (16). To formally test this possibility, we systematically reduced the expression of RhoA, Rac1, and Cdc42 protein levels using siRNA methods and tested the impact on TcdB-induced necrosis in HeLa and Caco2 cells. We found that cell death was independent of RhoA and Cdc42 expression levels, but dependent on the presence of Rac1 (Fig. 1).

The observation that the cell death pathway is specifically dependent on Rac1 suggests a pathway in which Rac1 is involved in the recruitment and assembly of the NOX complex (18). Assembly of the NOX complex on endosomes can result in the intracellular production of ROS, a condition that can be lethal to the cell (25). In concordance with this, TcdB stimulation resulted in a transient activation of Rac1 (Fig. 1*C*) and robust production of ROS in both cultured cells (Fig. 2*A*) and colon tissue explants (Fig. 4*A*). The levels of ROS (Figs. 2*A* and 4*A*) were inversely correlated with cell viability (Fig. 2*B*) and tissue architecture integrity (Fig. 4 *B–D*). ROS production precedes necrosis and is an early event postintoxication (Fig. 2*C*). These observations support a model in which intoxication with TcdB triggers the production of ROS, which ultimately accumulate at high levels and kill the cell.

Previous reports have noted oxidative stress pathways activated or up-regulated in response to *C. difficile* TcdA (26, 27), and NAC is known to modify the oxidative imbalance in TcdB-treated cells (28). Although many of the previous studies of TcdA have suggested that the oxidative stress is due to mitochondrial ROS production, the dependence on Rac1 led us to speculate that the primary driver of oxidative stress in response to TcdB is NOX-mediated. To test this hypothesis, we reduced the expression of various NOX complex components with siRNA and tested the impact on TcdB-mediated cell death. Our observation that NOX3 and NOX1 are the important components in HeLa and Caco2 cells, respectively, is consistent with their relative expression levels (Fig. 3 *A* and *B*). The high expression of NOX1 in Caco2 cells is consistent with in vivo observations of high NOX1 expression in the human gastrointestinal tract (29). Knockdown of p22phox expression conferred protection to TcdB in both cell types, consistent with the central role of p22phox in NOX complex assemblies (Fig. 3*A*). In addition to the siRNA approach, a series of ROS inhibitors and scavengers conferred significant protection against TcdB cytotoxicity (Fig. 3*D*). Although these inhibitors are not specific to the NOX flavocytochrome or NOX-derived ROS products, they do support the observation that the death pathway is driven by ROS production. The report of reactive nitrogen species (RNS) generated in the presence of toxin (30) is consistent with our observations, given that RNS and ROS can act synergistically to drive nitrosylation and lipid oxidation (31).

One paradoxical aspect of a Rac-dependent and NOX-mediated cell death mechanism is that TcdB is known to inactivate Rac through its glucosyltransferase activity. An explanation that addresses this apparent paradox is that Rac-dependent NOX assembly occurs during the process of TcdB entry into endosomes, before delivery of the TcdB glucosyltransferase domain. This idea is supported by the observation that Rac1 is activated immediately in response to the toxin (Fig. 1*C*) and is subsequently inactivated at later time points (Fig. 1*D*).

Recent work has highlighted the importance of redox signaling from the endosome (20). These redox active endosomes, termed "redoxosomes," are formed on receptor ligation and internalization via the clathrin-mediated endocytic route. The ligated receptor recruits active NOX to the site of vesicle formation. Because TcdB is internalized via a clathrin-mediated pathway (17), we speculate that ligation of TcdB receptor(s) triggers assembly of the NOX complex at the plasma membrane and leads to internalization of both TcdB and activated NOX. We propose that TcdB binds the cell surface and induces redoxosome formation, and that the resulting burst of intracellular superoxide generates the ROS and RNS that overpower endogenous antioxidant pathways, resulting in necrosis.

The mechanistic understanding of TcdB-mediated necrosis in cells motivated us to explore the role of TcdB-induced ROS in the context of physiologically relevant tissue. We have previously shown that doses of 10 or 100 nM TcdB induce tissue damage in the colonic explant model (16). In the present study, DPI treatment abrogated ROS production and conferred nearly complete protection against TcdB in the porcine colonic explant system (Fig. 4 *A–D*). This finding demonstrates that observations of oxidative stress-mediated necrosis in cultured cell lines can be extrapolated to systems that are more reflective of in vivo conditions.

Building on our DPI results, we next tested the antioxidant NAC. This compound is approved for therapeutic applications in humans and has a protective phenotype against toxin in tissue culture cells (Fig. 3*D*). In a human colonic explant model, NAC attenuated toxin-induced damage, even at high doses of toxin (Fig. 5). In both cells and tissue, NAC was not as effective as DPI, presumably because it acts in the final step in the pathway, after ROS have been generated in the cell. Nevertheless, this study provides proof of concept that chemical attenuation of ROS could serve as a viable strategy for protecting the colonic mucosa of patients with CDI.

TcdB hijacks a cellular defense pathway typically found in phagocytic cells and uses it to kill the host epithelial cell. Given that the effect of redoxosome activation is detrimental to the cell, we assume that TcdB is causing aberrant activation of the pathway. Considering that there are many physiological ligands of clathrin-linked receptors that do not result in NOX assembly and ROS production, we speculate that there are multiple TcdB receptors, and that TcdB pulls them together with the NOX complex in a unique way. In our view, the most important goal for future studies is to identify the cellular receptors for TcdB. Not only could these host factors serve as new targets for blocking the effects of TcdB, but also the receptor identity could provide insight into mechanisms of aberrant NOX activation and unregulated ROS production occurring in some forms of cancer, cardiovascular disease, neurodegenerative disease, and pancreatitis (32–36).

Methods

Recombinant Protein Production. Recombinant TcdA, TcdB, and TcdB D270N proteins were expressed in *B. megaterium* and purified as described previously (16).

Cell Lines, Inhibitors, and Viability Assays. HeLa cells were maintained in DMEM supplemented with 10% (vol/vol) FBS at 37 °C with 5% CO_2. Caco2 cells were cultured in MEM supplemented with 10% (vol/vol) FBS, 10 mM Hepes, 10 nM sodium pyruvate, and 1× MEM nonessential amino acids at 37 °C with 5% CO_2. Tempol (sc-200825; Santa Cruz Biotechnology) was resuspended in ethanol and used at 10 mM. DPI (D2926; Sigma-Aldrich) was dissolved in DMSO and used at a final concentration of 10 μM. The Rac1 inhibitor NSC 23766 (2161; Tocris Bioscience) and *N*-acetyl-L-cysteine (ENZ-51011; Enzo Life Sciences) were prepared in water and used at 1 mM and 5 mM, respectively. All inhibitors were added in complete media and incubated for 1 h at 37 °C before toxin challenge. Viability was measured at 16 h postintoxication using the CellTiter-Glo Luminescent Cell Viability Assay (G7573; Promega) according to the manufacturer's instructions. Necrosis was quantified by measuring LDH release in a luminescent assay using CytoToxGlo (G9290; Promega).

siRNA Transfection. siRNA transfection was performed using a reverse-transfection approach. In brief, siRNA (Thermo Scientific) was diluted to 100 nM in serum-free medium. RNAiMax (Life Technologies) was prepared in serum-free medium at 0.007 μL of RNAiMax/μL of medium, mixed with diluted siRNA 2:1, and incubated at room temperature for 15 min before being added to a 384-well plate at 15 μL/well, with six wells per target. Then 35 μL of 2.9×10^4 cells/mL was added to each well, followed by 48 h of

incubation at 37 °C. For each target, three wells received mock treatment and three wells received 50 nM TcdB for 16 h. Cytotoxicity was determined with the CellTiter-Glo Luminescent Cell Viability Assay. The average treated value was normalized to the average mock value to establish percent survival. The percent survival for each target was normalized to the percent survival of cells transfected with a luciferase (Luc) siRNA is shown. Transfection efficiency was monitored using AllStars Death siRNA, comparing viability with that of mock-treated Luc control.

RT-PCR and Western Blot Analysis. RNA was isolated and purified using the RNeasy Mini Kit (Qiagen), using 10 ng RNA per reaction. Targets were amplified with the OneStep RT-PCR Kit (Qiagen) using oligos listed in *SI Methods*. Cells were lysed in 50 mM Tris·Cl (pH 8), 150 mM NaCl, 1% TritonX-100, 0.5% sodium deoxycholate, and 0.1% SDS and then resolved on 12% SDS/PAGE gels. Immunoblots were probed with antibodies against Rac1 (clone 23A8; Millipore), RhoA (ARH-03; Cytoskeleton), Cdc42 (2462; Cell Signaling), p22phox (sc-20781; Santa Cruz Biotechnology), or tubulin (3873S; Cell Signaling). Binding of an anti-mouse (115-035-174; Jackson ImmunoResearch Laboratories) or an anti-rabbit (7074; Cell Signaling) HRP-conjugated secondary antibody was detected with the LumiGLO Kit (Cell Signaling) according to the manufacturer's instructions.

Rac1 Activation and Inactivation. HeLa cells were cooled to 4 °C for 1 h before the addition of 10 nM toxin for an additional 1 h at 4 °C. Cells were then shifted to 37 °C for the indicated time points and lysed for analysis. Rac1 activation was assayed using the G-LISA Rac1 Activation Assay Biochem Kit (BK125; Cytoskeleton). Relative activation was determined by comparing the signals from the toxin-treated sample with those from a mock-treated control at the corresponding time point. Rac1 glucosylation was assayed by Western blot analysis as described previously (16). The mock-treated samples served as controls.

ROS Detection. ROS were detected with the Total ROS Detection Kit (ENZ-51011; Enzo Life Sciences). Oxidative stress detection reagent was reconstituted in anhydrous dimethylformamide to yield a 5 mM stock solution. Then 5 μM detection reagent in complete media was added to each well of a 96-well plate for 1 h at 37 °C. Cells were washed twice with HBSS (cellgro 21-023-CV; Corning), and toxin was added in HBSS. Mock- treated and H_2O_2-treated (1 mM final concentration) cells were included as controls. Fluorescence was detected using a Synergy 4 plate reader with a 488/528 filter set. The average value for each treatment was normalized to the mock-treated wells to establish relative induction.

Colonic Explants. Animal husbandry and experimental procedures related to the porcine colonic explants were performed in accordance with Vanderbilt University's Institutional Animal Care and Use Committee (IACUC) policies. Discarded colon tissues were obtained from pigs after euthanization at the end of IACUC-approved animal use protocols and prepared for intoxication as described previously (16). Human colonic tissue was obtained by the Cooperative Human Tissue Network from consented, deidentified donors under Institutional Review Board-approved protocol 031078. ROS detection reagent and 10 μM DPI or DMSO mock treatment were added to tissue for 1 h at 37 °C. Tissue was challenged with 10 nM or 100 nM TcdB for 5 h at 37 °C. Frozen tissue sections were prepared by embedding in OCT compound (4583; Tissue-Tek) and snap-freezing in a dry ice bath. Sections were cut at the Vanderbilt University Translational Pathology Shared Resource Core. Slides were thawed and immediately analyzed with a Zeiss LSM 510 confocal microscope. The staining and scoring of tissues was performed as described previously and detailed in *SI Methods*.

ACKNOWLEDGMENTS. We thank Phil Williams of the Vanderbilt Light Surgical Laboratory for providing porcine tissue samples. This project was supported by Public Health Service Grant R01 AI095755 from the National Institutes of Health and the Burroughs Wellcome Foundation through an Investigators in the Pathogenesis of Infectious Disease Fellowship (to D.B.L.). Human tissue samples were provided by the Cooperative Human Tissue Network, which is funded by the National Cancer Institute. Core services performed at through Vanderbilt University Medical Center's Digestive Disease Research Center were supported by National Institutes of Health Grant P30DK058404.

1. Kelly CP, LaMont JT (2008) *Clostridium difficile*—more difficult than ever. *N Engl J Med* 359(18):1932–1940.
2. Bartlett JG (2002) Clinical practice: Antibiotic-associated diarrhea. *N Engl J Med* 346(5):334–339.
3. Voelker R (2010) Increased *Clostridium difficile* virulence demands a new treatment approach. *JAMA* 303(20):2017–2019.
4. Voth DE, Ballard JD (2005) *Clostridium difficile* toxins: Mechanism of action and role in disease. *Clin Microbiol Rev* 18(2):247–263.
5. Kuehne SA, et al. (2010) The role of toxin A and toxin B in *Clostridium difficile* infection. *Nature* 467(7316):711–713.
6. Lyras D, et al. (2009) Toxin B is essential for virulence of *Clostridium difficile*. *Nature* 458(7242):1176–1179.
7. Just I, et al. (1995) Glucosylation of Rho proteins by *Clostridium difficile* toxin B. *Nature* 375(6531):500–503.
8. Just I, et al. (1995) The enterotoxin from *Clostridium difficile* (ToxA) monoglucosylates the Rho proteins. *J Biol Chem* 270(23):13932–13936.
9. Jank T, Aktories K (2008) Structure and mode of action of clostridial glucosylating toxins: The ABCD model. *Trends Microbiol* 16(5):222–229.
10. Giesemann T, Egerer M, Jank T, Aktories K (2008) Processing of *Clostridium difficile* toxins. *J Med Microbiol* 57(Pt 6):690–696.
11. Donta ST, Sullivan N, Wilkins TD (1982) Differential effects of *Clostridium difficile* toxins on tissue-cultured cells. *J Clin Microbiol* 15(6):1157–1158.
12. Chaves-Olarte E, Weidmann M, Eichel-Streiber C, Thelestam M (1997) Toxins A and B from *Clostridium difficile* differ with respect to enzymatic potencies, cellular substrate specificities, and surface binding to cultured cells. *J Clin Invest* 100(7):1734–1741.
13. Krivan HC, Clark GF, Smith DF, Wilkins TD (1986) Cell surface binding site for *Clostridium difficile* enterotoxin: Evidence for a glycoconjugate containing the sequence Gal alpha 1-3Gal beta 1-4GlcNAc. *Infect Immun* 53(3):573–581.
14. Dingle T, et al. (2008) Functional properties of the carboxy-terminal host cell-binding domains of the two toxins, TcdA and TcdB, expressed by *Clostridium difficile*. *Glycobiology* 18(9):698–706.
15. Frisch C, Gerhard R, Aktories K, Hofmann F, Just I (2003) The complete receptor-binding domain of *Clostridium difficile* toxin A is required for endocytosis. *Biochem Biophys Res Commun* 300(3):706–711.
16. Chumbler NM, et al. (2012) *Clostridium difficile* Toxin B causes epithelial cell necrosis through an autoprocessing-independent mechanism. *PLoS Pathog* 8(12):e1003072.
17. Papatheodorou P, Zamboglou C, Genisyuerek S, Guttenberg G, Aktories K (2010) Clostridial glucosylating toxins enter cells via clathrin-mediated endocytosis. *PLoS ONE* 5(5):e10673.
18. Hordijk PL (2006) Regulation of NADPH oxidases: The role of Rac proteins. *Circ Res* 98(4):453–462.
19. Leto TL, Morand S, Hurt D, Ueyama T (2009) Targeting and regulation of reactive oxygen species generation by Nox family NADPH oxidases. *Antioxid Redox Signal* 11(10):2607–2619.
20. Oakley FD, Abbott D, Li Q, Engelhardt JF (2009) Signaling components of redox active endosomes: The redoxosomes. *Antioxid Redox Signal* 11(6):1313–1333.
21. Brown DI, Griendling KK (2009) Nox proteins in signal transduction. *Free Radic Biol Med* 47(9):1239–1253.
22. Dinauer MC, Orkin SH, Brown R, Jesaitis AJ, Parkos CA (1987) The glycoprotein encoded by the X-linked chronic granulomatous disease locus is a component of the neutrophil cytochrome b complex. *Nature* 327(6124):717–720.
23. Ambasta RK, et al. (2004) Direct interaction of the novel Nox proteins with p22phox is required for the formation of a functionally active NADPH oxidase. *J Biol Chem* 279(44):45935–45941.
24. Ueno N, Takeya R, Miyano K, Kikuchi H, Sumimoto H (2005) The NADPH oxidase Nox3 constitutively produces superoxide in a p22phox-dependent manner: Its regulation by oxidase organizers and activators. *J Biol Chem* 280(24):23328–23339.
25. Panieri E, et al. (2013) Reactive oxygen species generated in different compartments induce cell death, survival, or senescence. *Free Radic Biol Med* 57:176–187.
26. Qiu B, Pothoulakis C, Castagliuolo I, Nikulasson S, LaMont JT (1999) Participation of reactive oxygen metabolites in *Clostridium difficile* toxin A-induced enteritis in rats. *Am J Physiol* 276(2 Pt 1):G485–G490.
27. He D, et al. (2000) *Clostridium difficile* toxin A causes early damage to mitochondria in cultured cells. *Gastroenterology* 119(1):139–150.
28. Fiorentini C, Falzano L, Rivabene R, Fabbri A, Malorni W (1999) N-acetylcysteine protects epithelial cells against the oxidative imbalance due to *Clostridium difficile* toxins. *FEBS Lett* 453(1-2):124–128.
29. Suh YA, et al. (1999) Cell transformation by the superoxide-generating oxidase Mox1. *Nature* 401(6748):79–82.
30. Savidge TC, et al. (2011) Host S-nitrosylation inhibits clostridial small molecule-activated glucosylating toxins. *Nat Med* 17(9):1136–1141.
31. Sautin YY, Nakagawa T, Zharikov S, Johnson RJ (2007) Adverse effects of the classic antioxidant uric acid in adipocytes: NADPH oxidase-mediated oxidative/nitrosative stress. *Am J Physiol Cell Physiol* 293(2):C584–C596.
32. Block K, Gorin Y (2012) Aiding and abetting roles of NOX oxidases in cellular transformation. *Nat Rev Cancer* 12(9):627–637.
33. Lassègue B, San Martín A, Griendling KK (2012) Biochemistry, physiology, and pathophysiology of NADPH oxidases in the cardiovascular system. *Circ Res* 110(10):1364–1390.
34. Cairns B, Kim JY, Tang XN, Yenari MA (2012) NOX inhibitors as a therapeutic strategy for stroke and neurodegenerative disease. *Curr Drug Targets* 13(2):199–206.
35. Kim YJ, Kim EH, Hahm KB (2012) Oxidative stress in inflammation-based gastrointestinal tract diseases: Challenges and opportunities. *J Gastroenterol Hepatol* 27(6):1004–1010.
36. Guzik TJ, Griendling KK (2009) NADPH oxidases: Molecular understanding finally reaching the clinical level? *Antioxid Redox Signal* 11(10):2365–2370.